https://doi.org/10.1038/s44304-026-00175-x

Projections of tropical cyclone-driven storm-tide risk to critical infrastructure in the Bay of Bengal

Coleman P. Blakely[1] ✉, William J. Pringle[1] & V. R. Kotamarthi[2]

Due to its low elevation and densely populated coast, the Bay of Bengal (BoB) is uniquely vulnerable to tropical cyclone (TC)-driven storm-tides. This study uses a high-resolution, coupled hydrodynamic and wave model of the BoB to simulate several millennia of present and future climate synthetic tropical cyclones. We quantify nonlinear interactions among storm surge, tides, river discharge, and sea-level rise. While results reveal strong spatial variability, wave runup, tide-surge, and the interaction of mean sea levels and surge are the strongest of these processes. Using combinations of forcing states, we generate a dataset of storm-tide levels at sites of critical infrastructure and estimate long-term (>100-year) storm-tide return levels for present-day and mid-century conditions. Future scenarios project decreased flood risk across the eastern Ganges-Brahmaputra-Meghna delta but heightened risk along India's eastern coast, where the Kovvada Atomic Power Project may see up to a 78% increase in 5000-year storm-tide levels.

The Bay of Bengal (BoB) region is highly susceptible to tropical cyclone-driven storm-tide hazards due to its high population density and low-lying coastal zone. While the region accounts for only 7.8% of the total number of recorded surge events globally, the events that do occur are extremely strong, with an average of five surge events per decade exceeding 5 m[1]. These events imperil the estimated 170 million people in the region who live below 10 m of elevation[2]. Particularly at risk is the Northern BoB surrounding the Ganges-Brahmaputra-Meghna Delta (GBM), consisting of the Country of Bangladesh and the Indian State of West Bengal, where the complex hydrodynamics of the river delta and the risk of high-intensity tropical cyclones (TCs) greatly increase the risk of compound flooding[3].

In the next 25–30 years, coastal populations in the region—which includes large cities such as Kolkata, Chennai, and Visakhapatnam on the east coast of India; and Chittagong in Bangladesh—are expected to continue to grow[4,5]. Supporting these growing populations will require the construction of new infrastructure such as transportation networks, telecommunication services, electricity generation, and healthcare services. Failures and disruptions to this critical infrastructure can cascade, causing further suffering and damage in the wake of extreme storms[6,7]. At the same time as this population growth and infrastructure construction, the storm-tide hazard in the BoB will be exacerbated by higher-intensity cyclones[8], subsiding river deltas[9,10], and rising sea levels.

Accurately predicting storm-tide risk under present and future conditions is critical to provide policy makers and risk managers with the information they require to both protect existing assets (power plants, hospitals, etc.) and to inform the siting of additional infrastructure required to support a growing population base. In the BoB, this aim is complicated by several factors, including the strong riverine influence of the GBM system, rapidly evolving deltaic topobathy, and limited long-term observations of coastal water levels[11] in the region. This complex marginal sea necessitates physics-based modeling approaches that are capable of resolving nonlinear interactions between oceanic, hydrologic, and atmospheric processes. Such nonlinear phenomena, such as tide-surge interaction, can greatly alter storm-tides and are best resolved using physics-based models.

To address this need, a substantial body of work advancing understanding of tides, storm surge, and coastal flooding in the BoB can be found in the literature. For example[12], showcases an improved bathymetric dataset for the GBM delta, validating their new topographic/bathymetric dataset with tidally-forced hydrodynamic simulations of the region and showing the importance of accurately resolving the complex coastal region. Additional studies have examined specific storm events, performing hindcasts of some of the most devastating TCs to hit the region [refs. 13–16, among others]. Complementary works have analyzed flood return periods in the region under both present and future climate conditions[17–22], while others have examined the interaction of different processes—e.g., the interactions between riverine discharge, wind-driven surge, and rainfall[23]; or the contribution of wave radiation stress on storm-surge on the East Coast of

[1]Environmental Science Division, Argonne National Laboratory, Lemont, IL, USA. [2]Decision and Infrastructure Sciences, Argonne National Laboratory, Lemont, IL, USA. ✉e-mail: cblakely@anl.gov

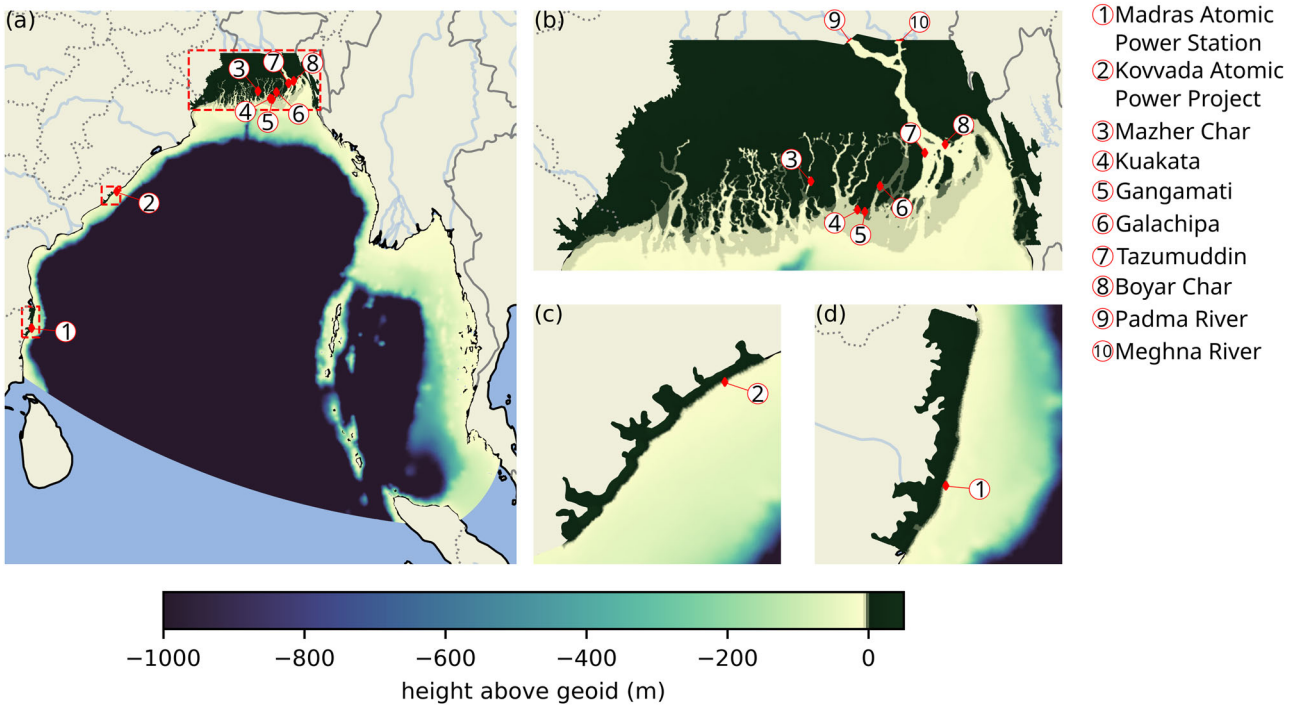

Fig. 1 | Computational mesh covering the Bay of Bengal with sites of interest labeled. a Computational mesh domain with reactor sites indicated by red diamonds and labeled with numbers; **b–d** Insets of high-resolution regions with flood plains. River inflow boundary conditions are denoted by the red solid lines.

India[24]. Clearly, assessing coastal hazards in this highly populated and developing region is an active area of research.

These aforementioned studies underscore the importance of nonlinear coastal and hydrologic processes, however, they generally focus on specific events, use relatively few ensemble members in their extreme value analyses, or focus only on specific interactions/drivers of storm-surge. For example[20], incorporated tidal forcing in their simulation of several thousand synthetic TCs; however, only one tidal stage per storm was accounted for, while[21] excluded tidal forcing in order to isolate the impact of changes in storm behavior at the mid-century. These design choices limit the ability to attribute storm-surge to different drivers and do not allow for great confidence in long-term (>100-year) return levels.

In this study, we present a high-resolution, fully coupled ADvanced CIRCulation (ADCIRC) and Simulated WAves Nearshore (SWAN)[25–27] modeling framework of the BoB. Using this model, we simulate both present-day and mid-century climate conditions using one historical and four future climate realizations each containing a millennia's worth of tropical cyclones. For each storm, multiple tidal and riverine perturbations are applied, for future climate scenarios mean sea level is accounted for, and the effects of waves are incorporated through the coupling to SWAN in order to sample nonlinear interactions. Projections of mean sea level rise are also considered for the future climate scenarios. The resulting ensemble is used to estimate long-term tropical cyclone-driven storm-tide water levels at sites of critical coastal infrastructure in the BoB. Storm-tide is defined here as the total water level resulting from the combined effects of meteorologically driven surge, astronomical tides, riverine discharge, and mean sea level. Long-term return levels are estimated via fitting of the Generalized Pareto Distribution (GPD) with a peaks-over-threshold (POT) extreme value approach. In addition to the full storm ensemble, singly-forced simulations of tides, meteorology-only storm-surge, and riverine discharge are performed and used to assess the relative importance of nonlinear processes such as tide-surge interaction and wave-related contributions. This is accomplished via a regression-based sensitivity analysis that is intended for diagnostic attribution rather than event-level prediction and allows for the relative importance of various physical processes in estimating storm-tide hazards. While we apply this methodology specifically to sites of existing or proposed nuclear power plants in the region, it is applicable to any coast and region where storm-tide risk assessment would be useful. Furthermore, the storm-tide return levels reported hold true for the areas immediately surrounding the points of interest.

The remainder of this manuscript is structured as follows. First, we present the results of both our sensitivity analysis and calculated return levels for long return periods (Results). Next, we discuss the results of this study as well as future paths of inquiry presented by our findings ("Discussion"). Detailed information on model setup and methods, namely the hydrodynamic model, including mesh generation, model forcing, and validation, as well as an explanation for how return levels were calculated, are explained in "Methods".

Results

This section presents the results from the two complementary analyses designed to examine tropical cyclone-driven coastal flood risk—expressed in terms of extreme storm-tide water levels—in the Bay of Bengal. Specifically, we (1) diagnose the importance of nonlinear interactions among storm-tide drivers using a regression-based comparison to linear superposition, and (2) estimate long-period storm-tide return levels under present and mid-century scenarios using extreme value analysis. The computational domain with topo/bathy and sites of interest labeled is shown in Fig. 1. All of the analyses and results are based on event-maximum storm-tides. In this study, "storm-tide" is defined as the maximum simulated total water level at a site of interest and includes the effects of meteorologically driven surge, astronomical tides, wave radiation stress, riverine discharge, and mean sea level offset. To compute this value, we take the maximum water level over all mesh nodes within 5 km of each site.

The synthetic storms used are generated using the Synthetic Tropical cyclOne geneRation Model (STORM) algorithm[28]. The millenia corresponding to present-day conditions statistically matches samples from the International Best Track Archive for Climate Stewardship (IBTrACS)[29,30], while the four millenia for future climate scenarios are

drawn from four mid-century climate models from the Climate Model Intercomparison Project version 6 (CMIP6)[31,32]. Each synthetic storm is simulated using a fully coupled ADCIRC+SWAN model of the BoB. Coupling to SWAN allows wave effects (via wave radiation stresses) to be physically represented in all simulations used for extreme value analysis. Nonlinear interactions between different forcing mechanisms are sampled by simulating each storm 12 times, with four tidal phases—low tide, high tide, maximum flood current, maximum ebb curent—at landfall and three riverine discharge states—minimum, maximum, and mean mean monthly calculated from reanalysis from the Global Flood Awareness System (GloFAS)[33]. Mid-century storms additionally have a spatially-varying mean sea level offset interpolated from Deltares Global Tide and Surge Model version 3.0 (GTSM)[34] enforced at the open ocean boundary. In addition to the full ensemble simulations, additional auxiliary simulations were performed to estimate the relative importance of nonlinear interactions through comparison of the full ensemble results to linear superposition of the auxiliary simulations. These include simulations of each individual storm in a "baseline" configuration forced only by meteorological fields and mean mean monthly riverine discharge as well as five single-forcing simulations to isolate the individual contributions of tides, riverine discharge, and mean sea level:

- Tide-only forcing with mean mean monthly riverine discharge (present climate)
- Tide-only forcing with mean mean monthly riverine discharge and mid-century mean sea level offset
- Minimum mean monthly riverine discharge
- Mean mean monthly riverine discharge
- Maximum mean monthly riverine dischargeThese auxiliary simulations are not part of the storm ensemble, but are used exclusively to perform the sensitivity analysis described in "Sensitivity analysis".

The long-term return levels reported in "Extreme Value Analysis" are estimated for each climate scenario using the full ensemble simulations and a Generalized Pareto Distribution (GPD) with Peaks Over Threshold (POT) approach. Uncertainty is quantified via bootstrap resampling. Detailed descriptions of the ADCIRC+SWAN model, forcing sources, and statistical methodology are found in "Methods".

Sensitivity analysis

To quantify the relative contributions of the nonlinear interactions among storm surge, tides, riverine discharge, and mean sea level, we compare the total water levels from the full storm ensemble to estimates based on linear superposition. Differences between the linear superposition and the full ensemble water levels are interpreted as the combined effect of nonlinear physical processes such as tide-surge interaction and wave setup. These effects are estimated using a regression framework defined as:

$$\begin{aligned}\eta_{twl} &= \eta^*_{baseline} + \eta_{tide} + \eta_{river} + \eta_{msl} + \alpha_1\eta^*_{baseline} \\ &\quad +\alpha_2\eta^*_{baseline}\eta_{tide} + \alpha_3\eta^*_{baseline}\eta_{river} + \alpha_4\eta^*_{baseline}\eta_{msl} \\ &\quad +\alpha_5\eta_{tide}\eta_{river} + \alpha_6\eta_{tide}\eta_{msl} + \alpha_7\eta_{river}\eta_{msl}\end{aligned} \quad (1)$$

Where $\eta^*_{baseline} = \eta_{baseline} - \eta_{msl}$, in which $\eta_{baseline}$ is the water level from the storm's baseline simulation and η_{msl} is the water level due to mean sea level; η_{river} is the water level due to the riverine discharge; and α_i is a coefficient found by performing a least squares regression at a location of interest for all storms in the ensemble. η_{msl} is calculated as the zero-frequency harmonic constituent from the yearlong tide-only simulations. Because the baseline simulations include the mean mean monthly riverine discharge, η_{river} is calculated from the river-only simulations as $\eta_{river} = \eta_{river,flowstate} - \eta_{river,meanflow}$ (i.e., $\eta_{river} = 0$ for η_{twl} perturbations with mean riverine discharge). Note that in this formulation it is assumed that η_{twl} is equal to the linear superposition of $\eta_{baseline}$, η_{tide}, and η_{river} plus the nonlinear interactions between surge, tide, and riverine forces as well as the $\alpha_1\eta^*_{baseline}$ term, which we assume is a proxy for unresolved processes such as wave setup, which is not included in the baseline simulations.

In order to assess the relative importance of each α term in Eq. (1), we use the method of standardized coefficients. By standardizing both the dependent and independent variables prior to performing the least squares regression, we can calculate so-called beta coefficients. By combining the terms in Eq. (1) without α coefficients on the left hand side and standardizing:

$$\begin{aligned}\overline{\Delta\eta} &= \beta_1\overline{\eta^*_{baseline}} + \beta_2\overline{\eta^*_{baseline}\eta_{tide}} + \beta_3\overline{\eta^*_{baseline}\eta_{river}} + \beta_4\overline{\eta^*_{baseline}\eta_{msl}} \\ &\quad +\beta_5\overline{\eta_{tide}\eta_{river}} + \beta_6\overline{\eta_{tide}\eta_{msl}} + \beta_7\overline{\eta_{river}\eta_{msl}}\end{aligned} \quad (2)$$

Where,

$$\begin{aligned}\Delta\eta &= \eta_{twl} - \eta^*_{baseline} - \eta_{tide} - \eta_{river} - \eta_{msl} \\ \bar{Y} &= \frac{Y - \frac{1}{N}\sum_{i=1}^{N} Y_i}{\sigma(Y)} \\ N &= \text{Number of samples} \\ \sigma(Y) &= \text{Standard deviation of } Y \\ \beta_i &= \text{Standardized coefficient}\end{aligned}$$

The resulting β coefficients provide a sense of the relative importance of each nonlinear term in Eq. (1). Positive (negative) β values indicate that a given interaction term tends to increase (decrease) peak storm-tide relative to linear superposition.

Table 1 shows the correlation coefficients of various estimates of η_{twl}. As the table shows, the performance of the "Full Fit" (Eq. (1)) outperforms both the pure linear superposition (Fit 1), as well as Fit 2, which incorporates unresolved physics such as wave setup by including $\alpha_1\eta^*_{baseline}$, i.e., $\eta_{twl} = \eta^*_{baseline} + \eta_{tide} + \eta_{river} + \eta_{msl} + \alpha_1\eta^*_{baseline}$. The degradation seen between Fits 1 and 2 confirms that wave setup is not the sole contributor to larger storm surge when comparing η_{twl} and $\eta_{baseline}$, and that other nonlinear terms are required to accurately assess the contribution of various forces on storm-tides in the BoB.

The beta-coefficients of performing a least squares regression on Eq. (2) for each location of interest over all scenarios, storms, and perturbations are shown in Table 2 and Fig. 2. The magnitude of the coefficient provides a sense of the relative importance of each interaction term.

The effect of wave setup—approximated by the $\beta_1\overline{\eta^*_{baseline}}$ term—is generally larger for the locations on the east coast of India (Madras Atomic Power Station and Kovvada Atomic Power Project) as well as for locations towards the center/east of the GBM Delta (Gangamati and Mazher Char). On the other hand, the stations further west and upriver (Galachipa, Tazumuddin, Boyar Char) have smaller β_1 coefficients and the effect of wave setup on total water levels. The outlier of this pattern is Kuakata, located around 10 km west of Gangamati, but with a significantly lower β_1 coefficient.

Table 1 | Correlation coefficients (R^2) of estimates of η_{twl}

Location	Fit 1	Fit 2	Full Fit
Madras atomic power station	0.63	0.58	0.78
Kovvada atomic power project	0.82	0.65	0.86
Gangamati	0.84	0.85	0.94
Mazher Char	0.90	0.94	0.95
Boyar Char	0.80	0.81	0.95
Tazumuddin	0.85	0.84	0.95
Galachipa	0.93	0.90	0.96
Kuakata	0.86	0.86	0.93

Fit 1 compares η_{twl} with the linear superposition of $\eta^*_{baseline} + \eta_{tide} + \eta_{river} + \eta_{msl}$. Fit 2 additionally incorporates the effects of wave setup into the linear superposition by adding $\alpha_1\eta^*_{baseline}$. The "Full Fit" is that described in Eq. (1).

Table 2 | Standardized coefficients β_i for the terms in Eq. (2)

Location	β_1	β_2	β_3	β_4	β_5	β_6	β_7
Madras atomic power station	0.57	−0.24	-0.00	-0.27	-0.03	-0.28	0.03
Kovvada atomic power project	0.90	−0.53	0.00	−0.43	−0.01	−0.10	0.01
Gangamati	0.13	−0.60	−0.01	0.08	−0.04	−0.23	0.07
Mazher Char	0.08	−0.17	0.00	−0.27	0.02	0.08	−0.02
Boyar Char	−0.10	−0.49	−0.02	0.18	−0.02	−0.40	0.19
Tazumuddin	−0.09	−0.50	−0.01	0.10	−0.03	−0.34	0.22
Galachipa	−0.18	−0.45	−0.02	0.25	−0.03	−0.27	0.05
Kuakata	0.10	−0.54	−0.01	0.09	−0.05	−0.21	0.06

The β coefficient associated with tide-surge interaction (β_2) has a large magnitude for every site except Mazher Char. Mazher Char is located further inland and deeper in the GBM delta, likely resulting in less interaction between tides and surge. The remaining sites, however, all have β_2 coefficients with large magnitudes, highlighting the importance of not only including tides in simulations of TC-induced flooding but also that altering the tidal stage with respect to landfall can greatly change the resulting surge.

In more concrete terms, the impact of wave setup and the nonlinear interactions between tides, meteorologically driven storm surge, and riverine flow often result in different return levels at sites of interest. Figure 3 shows the change in 1000- and 5000-year return levels for all five climate realizations as compared to the full model ensemble for both the linear superposition fit (Fit 1), as well as when the effects of waves are approximated by adding $\alpha_1 \eta^*_{baseline}$ (Fit 2). While the effect of the nonlinear interactions between surge/tides/river currents varies depending on location and the climate model used, using linear superposition can result in return levels up to 25% lower than the full model ensemble. Conversely, by including only the effect of wave setup (superposition+waves), return levels up to 35% higher than the full model ensemble are calculated. These higher return levels are especially noticeable on the east coast of India at the Madras atomic power station and Kovvada atomic power projects. The reason that including only waves increases these return levels so drastically is that it does not capture the tide-surge interaction, which has a lowering effect on water levels in the region. It is vital to highlight that the purpose of this analysis is diagnostic rather than predictive. The regression framework is used only to rank the relative importance of the interaction terms and is not an attempt to reconstruct individual storm events.

Extreme value analysis

Storm-tide return levels at each site of interest are estimated using the full storm ensemble, and the extreme value analysis framework detailed in "Extreme value analysis methodology". Figure 4 shows the return level curves for return periods of 10–5000 years for the five climate realizations. Shaded bands indicate the 90% confidence interval. Figure 5 shows the 1000- and 5000-year return levels at sites of interest for both the present climate and the mean of the four return levels calculated from the CMIP6 scenarios.

Generally, long-term return levels decrease in the GBM Delta but increase along the east coast of India. In the GBM Delta, Boyar Char (Fig. 4e), and Tazumuddin (Fig. 4f) both exhibit lower—but still substantial—flood levels for return periods longer than 500 years. Further west, Galachipa (Fig. 4g), Gangamati (Fig. 4c), and Kuakata (Fig. 4h) see more modest but still noticeable decreases in long-term return levels, with the Hadgem scenario at Gangamati predicting an increased return level for return periods greater than ~2000 years. On the east coast of India, both the Madras Atomic Power Station (Fig. 4a), and Kovvada Atomic Power Project (Fig. 4b) see an increase in return level for all future climate scenarios. Finally, Mazher Char (Fig. 4d), located further inland in the middle of the GBM delta sees reductions in return levels under future conditions akin to those seen at the Tazumuddin and Boyar Char to the east.

While, generally speaking, the return levels on the GBM delta under these four future climate projections decrease, they are still substantial. For example, at Tazumuddin, the 1000-year return level under present climate conditions is around 8 m of storm-tide, while the mean of the four future climate scenarios predict a 1000-year return level of approximately 5 m. With the exception of Mazher Char, the sites on the GBM delta all see decreased return levels for both 1000- and 5000-year return periods of around 30% which, while substantial, still means that the 1000- and 5000-year storms would produce around 5 and 6.5 m of storm-tide respectively at Boyar Char, Tazumuddin, Galachipa, Gangamati, and Kuakata under mid-century conditions. In stark contrast, the Madras Atomic Power Station and Kovvada Atomic Power Project see increases in 1000-year (5000-year) return levels of 30 cm (50 cm) and 80 cm (1.5 m) or 16% (24%) and 47% (78%), respectively.

Across the GBM delta, projected decreases in return levels are consistent with changes in the STORM synthetic cyclone climatology, including fewer storms in several future realizations and shifts in genesis/track density toward the eastern Indian coast[35]. These changes reduce the frequency of high-intensity landfalling cyclones in the delta region.

To contextualize these changes in return levels, major historical cyclones in the region were simulated, and results were compared to our calculated return levels. Table 3 shows the equivalent return periods for the present and future scenarios of the largest historical storm surge at each reactor site based on these simulations. Cyclone Sidr was a category 4 TC which made landfall in Bangladesh in November of 2007. One of the deadliest storms to hit Bangladesh, Sidr is estimated to have resulted in at least 3447 deaths and caused $2.31 billion worth of damage[36]. The storm-tide caused by Sidr at Gangamati, Boyar Char, Tazumuddin, Galachipa, and Kuakata is the largest from the historical simulations and equivalent to a 70- to 210-year event under present climate conditions at those sites. Based on the future scenarios from the STORM dataset, storm-tides as extreme as those caused by Sidr would remain as uncommon or become far less common under future climate, with return periods ranging from 70 to over 3000 years. This aligns with the analysis from this study as well as observations of decreased cyclone intensity in the GBM delta from ref. 35.

The Kovvada Atomic Power Project faces an increased future risk from storm-tide-induced flooding. The 1.71 m surge at Kovvada was caused by the category 4 Cyclone Hudhud in October of 2014, which, based on this study, corresponds to a 1190-year storm under present climate conditions. Located approximately 70 km north of Vishakhapatnam, which saw an observed storm-tide of approximately 2 m during Hudhud, the Kovvada site can expect this level of surge to have a return period between 60 and 350 years under future climate conditions. The remaining two sites (Mazher Char and the Madras Atomic Power Station) do not appear to have drastically changing return periods/levels under future climate conditions; however, the maximum surges from the historical storms simulated in this study (Thane and Aila) were not the result of particularly powerful storms. Cyclone Thane was a category 2 storm which occurred in 2011, making landfall approximately 100 km south of the Madras Atomic Power Station while Cyclone Aila maxed out at category 1 winds and made landfall approximately 150 km to the west of Mazher Char.

Discussion

In this study, we estimate storm-tide return periods on the order of hundreds to thousands of years at sites of critical infrastructure in the BoB. Using the STORM dataset, we simulated a thousand years of TCs under five different climate conditions and quantified the influence of tides, riverine discharge, mean sea level rise, and their nonlinear interactions on extreme coastal water levels. We show that using simple linear superposition to estimate the effects of flooding due to storm-driven surge, tides, and riverine flow gives between −20% to +40% differences in the estimates of long-term return levels (1000–5000 years). Commensurate with other studies[24], we find that the impact of wave runup has the largest relative impact on

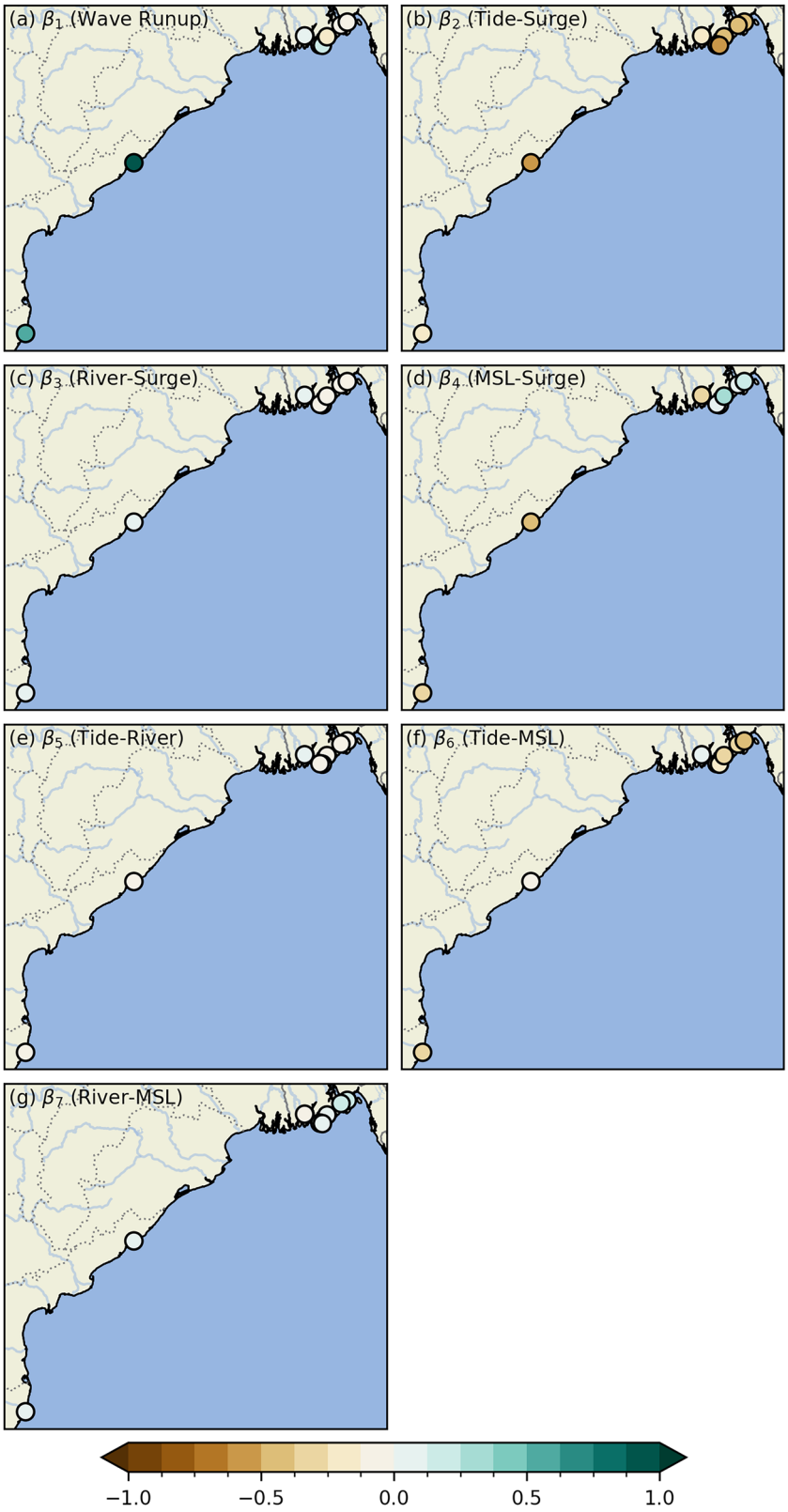

Fig. 2 | Standardized β coefficients denoting relative importance of interaction terms on storm-tides. Relative importance of various nonlinear interaction terms on storm-tides based on the regression analysis described by Eq. (2). Positive (negative) β coefficients indicate that a particular interaction term increases (decreases) storm-tides. The magnitude of β provides a sense of the relative importance of an interaction term. Interaction terms are: **a** Wave-setup; **b** tide-surge; **c** river-surge; **d** mean sea level-surge; **e** tide-river; **f** tide-mean sea level; **g** river-mean sea level.

increasing storm-tides as compared to linear superposition—especially along the east coast of India—the nonlinear interactions between tides and surge; mean sea levels and surge; and tides and mean sea levels are substantial and must be considered. While the numerical cost to simulate an ensemble of conditions for each storm is far from negligible, the potential difference in predicted return level has the potential to impact both the design of and decisions made regarding critical infrastructure. Moreover, reduced-order models, like the linear model described in "Sensitivity analysis", offer a potential pathway to simulate much larger storm ensembles.

Of particular interest is the finding that—based on the scenarios used by STORM—the eastern GBM delta sees a lower risk from TC-induced flooding under future scenarios, while the eastern coast of

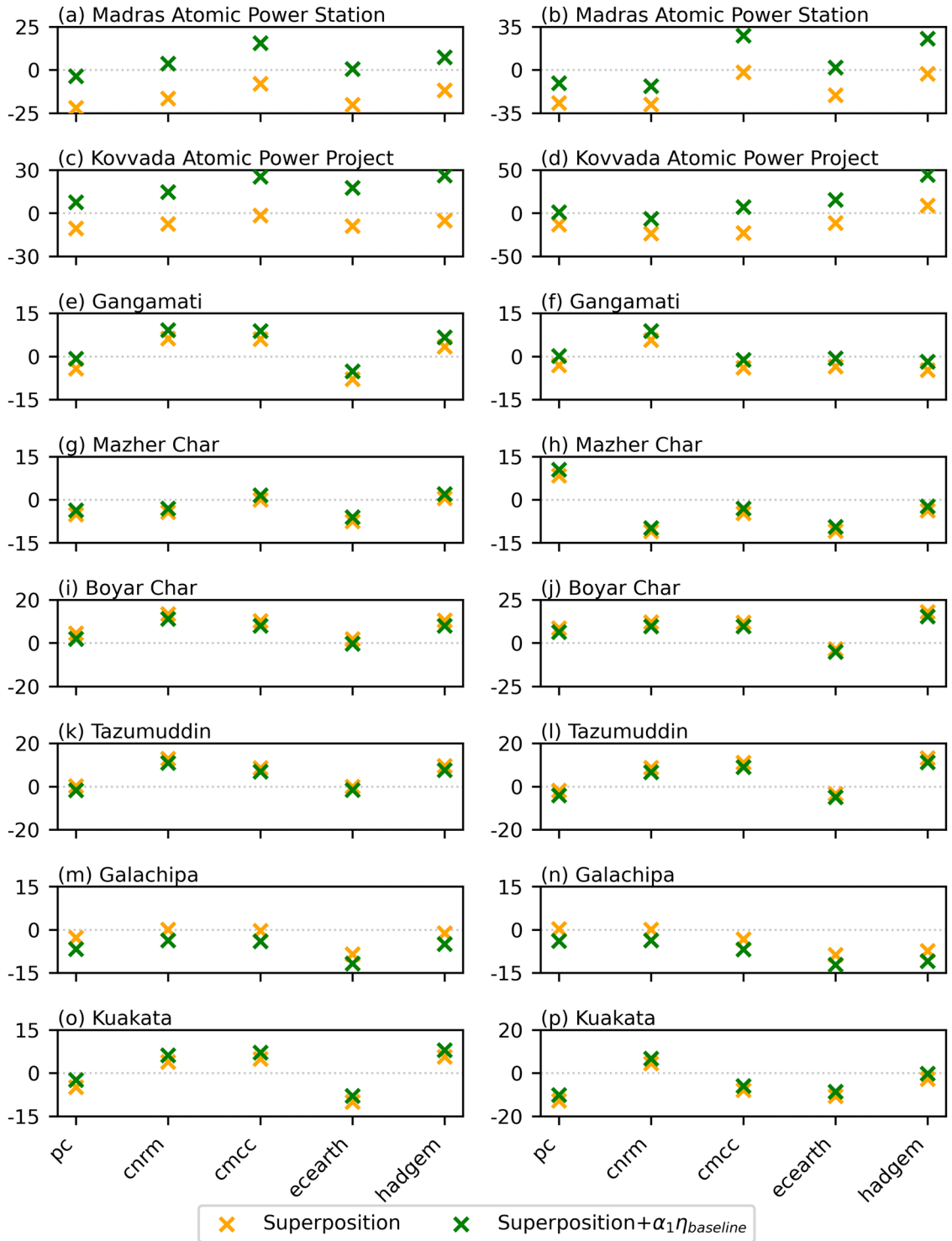

Fig. 3 | Comparison between 1000- and 5000-year return levels computed using the "full" model ensembles, linear superposition, and linear superposition + $\alpha_1\eta_{baseline}$. Left column shows the % difference between superposition (orange "X" markers) and superposition + $\alpha_1\eta_{baseline}$ (green "X" markers) compared to the full ensemble 1000-year return levels. The right column shows the same for 5000-year return levels. **a** and **b** show difference at the Madras Atomic Power Station; **c** and **d** at the Kovvada Atomic Power Project; **e** and **f** at Gangamati; **i** and **j** at Boyar Char; **k** and **l** at Tazumuddin; **m** and **n** at Galachipa; and **o** and **p** at Kuakata.

India sees increases in risk due to storm-tides. These regional contrasts, even within the relatively small BoB, highlight the need for region-specific flood risk assessments when siting and designing coastal infrastructure.

The projected decrease in long-term return levels in the GBM delta is consistent with changes in synthetic storm occurrence and intensity in the STORM dataset. As noted in ref. 35, shifts in cyclogenesis in the BoB cause tropical cyclone to drift west, towards the eastern coast of India. This shift reduces the intensity that cyclones are able to attain prior to landfall as well as decreases the number of cyclones which make landfall in the GBM delta. In contrast, the east coast of India sees increased positive contributions to storm-tide from wave setup and a weaker negative tide-surge interaction than on the delta, contributing to increased storm-tide hazard at the mid-century.

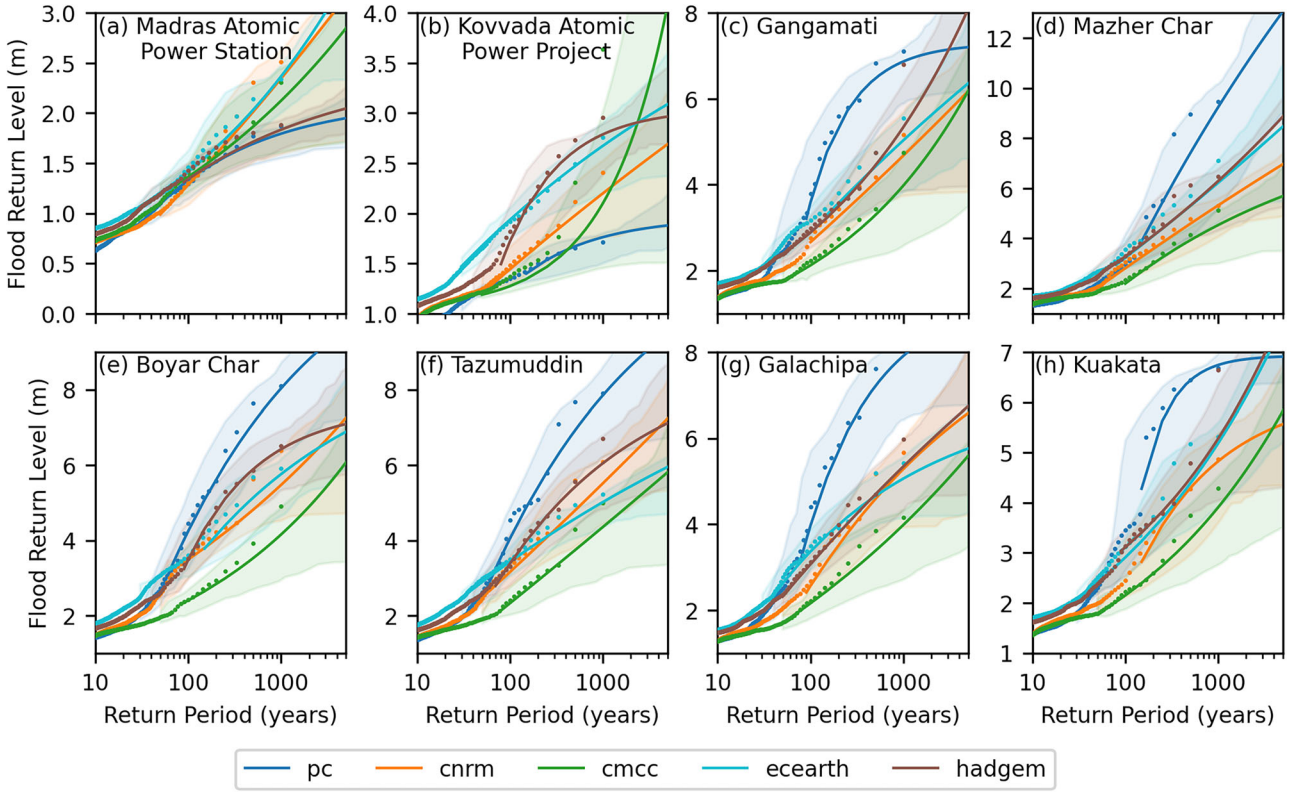

Fig. 4 | Calculated storm-tide return levels from the full model ensemble at sites of interest under all five climate realizations. Return levels as calculated from the full model ensemble for: **a** Madras Atomic Power Station; **b** Kovvada Atomic Power Project; **c** Gangamati; **d** Mazher Char; **e** Boyar Char; **f** Tazumuddin; **g** Galachipa; and **h** Kuakata. Solid lines show the storm-tide return levels calculated from the full model ensemble using the Generalized Pareto Distribution with Peaks Over Threshold for present climate (dark blue); cnrm (orange); cmcc (green); ecearth (light blue); and hadgem (brown). 90% confidence intervals calculated via bootstrapping are denoted by the background fill. Point data shows the (mean) empirical return level calculated from the full model ensemble.

Consistent with ref. 35, the STORM dataset finds that the GBM is one of two regions which have lower wind speeds under future climate scenarios. Other CMIP6 scenarios (or other algorithms for creating synthetic storms) could yield different return level predictions in the region[22]. The same holds true for the eastern coast of India, where we find generally higher risk due to storm-driven surge under the future climate. Other inputs to the ADCIRC +SWAN model also introduce uncertainty in the output. As described in "Methods", riverine inflow was calculated from the historic record and does not take into account potential changes in the behavior of tributaries to the GBM delta that may have occurred by mid-century. If, for example, riverine flow were to drastically increase due to large amounts of precipitation, the calculated return levels at locations near the river could change. Additionally, the effects of land subsidence—which was not included in this study—would doubtless change return levels, particularly in the northern and eastern part of the BoB in Bangladesh, where subsidence rates of 1–7 mm per year have been observed[10]. More accurate predictions of riverine flow, as well as changes in mean sea level, and higher fidelity bathymetry, which accounts for future land subsidence, would all increase confidence in predicted return levels.

Future directions of inquiry for this work could include finding numerically efficient methods to simulate the remaining ~45,000 years of STORM synthetic cyclones. Running a larger number of storms would greatly increase confidence in the return levels and allow for more meaningful prediction of up to the 10,000-year storm. Such approaches include reducing the number of perturbations of each storm via analysis of the β coefficients calculated in "Sensitivity analysis". For example, the small values of β_3 at every site of interest indicate that there is little interaction between riverine flow and storm-tide, indicating that eliminating riverine flow perturbations may not drastically change predicted return levels. Additionally, more refined machine learning methodologies could be applied to the large amount of data already generated in this study and could be used to create an "emulator" of the full ADCIRC+SWAN model, which would allow for more rapid simulation of large amounts of storms. In addition to the remainder of the STORM dataset, other synthetic track datasets for the region, e.g., ref. 22, CMIP6 climate products, and reanalysis/forecasting products such as ERA5[37] could be used to force the numerical model. By using a more diverse set of wind products, more confidence in the predicted return levels will exist. Perhaps the most impactful improvement that could be made would be the inclusion of land subsidence in future climate simulations.

Our results highlight the importance of incorporating region-specific, high-resolution modeling frameworks into flood risk assessments for coastal infrastructure. As changing conditions result in different flood risks in coastal zones, the importance of integrating these findings into infrastructure design and disaster preparedness strategies becomes paramount. The demonstrated variability in flood risks across even the relatively small region of the BoB highlights the importance of localized analyses to account for nonlinear interactions between tides, storm surge, riverine discharge, and sea level rise.

Methods

Hydrodynamic model

For this study, version 56 of the ADCIRC model[25,26,38] was used to perform hydrodynamic simulations of storm-tide and flooding. ADCIRC is a finite-element-based model that solves the Generalized Wave Continuity Equation (GWCE)[39], a reformulation of the shallow water equations, on unstructured, triangle-based computational meshes. ADCIRC is widely used in modeling both tides and storm surge in coastal zones [e.g., refs. 40–42, among others]. In order to model wave-current interaction and the resultant wave setup, ADCIRC is coupled with the SWAN model[27,43].

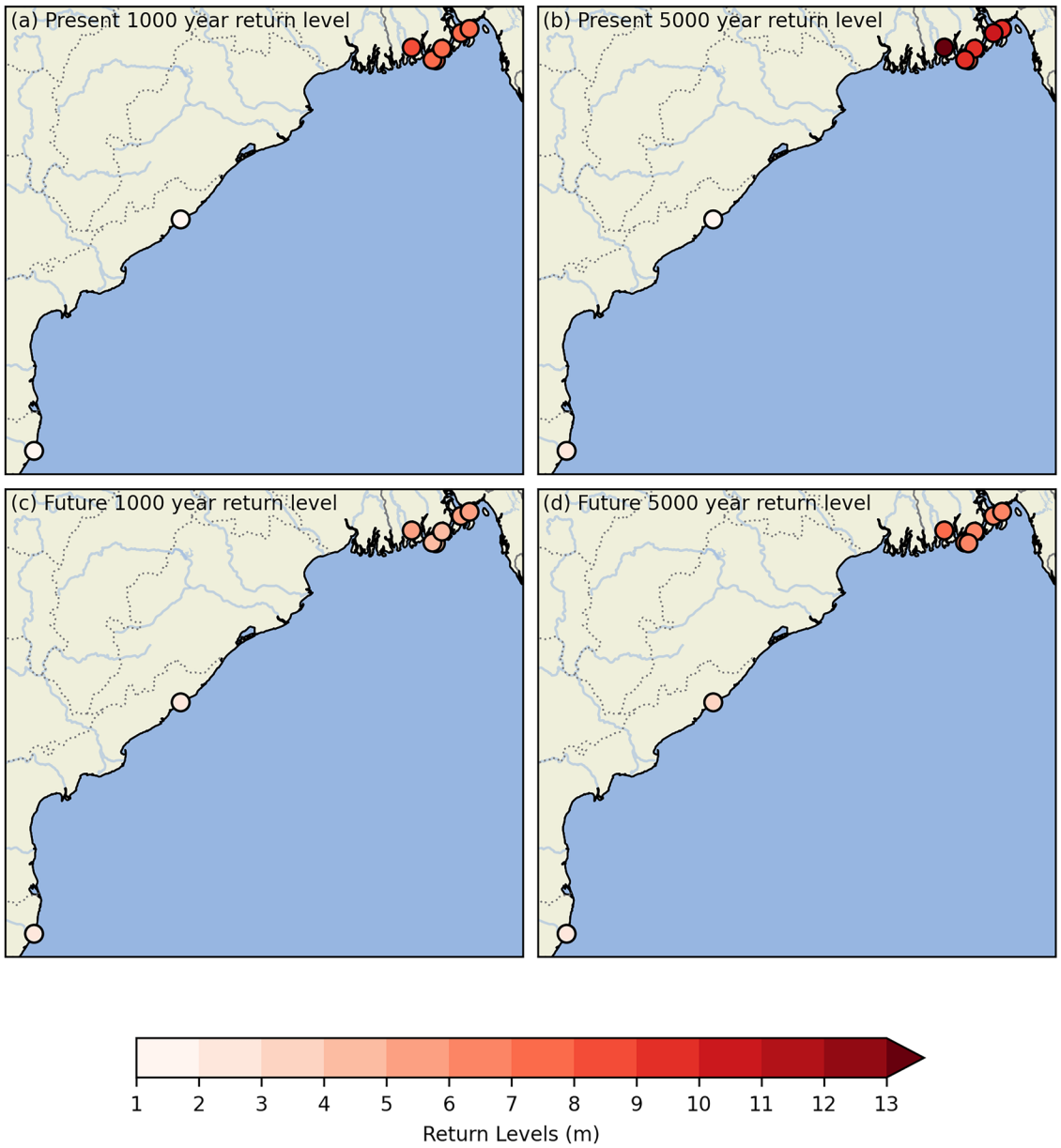

Fig. 5 | 1000- and 5000-year storm-tide return levels at sites of interest for present and (mean) future climate as calculated via the full model ensemble. a, **b** show the 1000-year (5000-year) storm-tide return levels at sites of interest as calculated from the full model ensemble. **c**, **d** show the 1000-year (5000-year) mean storm-tide return levels across the four future climate scenarios (cnrm, cmcc, eceaerth, hadgem) as calculated from the full model ensemble.

SWAN is a spectral wave model that solves the action-balance equation. Both ADCIRC and SWAN are run on the same unstructured computational mesh.

ADCIRC simulations used a time step of 5 s, temporal weighting in the GWCE of 0.05 s^{-1}, and the Smagorinsky closure model[44,45] with a lateral mixing coefficient of 0.2. SWAN was simulated using a time step of 10 min and coupled to ADCIRC at every SWAN time step. SWAN has additional dimensions for wave frequency and direction. The frequency range is discretized on the interval [0.031384, 1.420416] Hz using 41 bins with 36 directional bins (i.e., 10 degree spacing).

Model forcing

In order to capture nonlinear effects caused by the interaction of different water-level drivers, we run ADCIRC + SWAN forced with meteorology (surface winds and atmospheric pressure), astronomical tides, riverine discharge, and sea level rise. In this section, we detail our implementations of each of these forcings within the hydrodynamic model.

The STORM data set consists of 10,000 years of synthetic TCs. Each storm consists of the location of the center of the storm, the minimum atmospheric pressure, the maximum wind speed, and the radius of maximum winds at three-hourly time intervals. Timing information is limited to a year (from 0 to 9999) and the month during which the storm occurred. For present conditions (pc), STORM samples from the International Best Track Archive for Climate Stewardship (IBTrACS)[29], covering the years 1980–2018. The resulting synthetic TC tracks match the statistical distribution of the 38 years of observed TCs[30]. Mid-century (2015–2050) scenarios, apply STORM to four different CMIP6 models: CMCC-CM2-VHR4 (cmcc), CNRM-CM6-1-HR (cnrm), EC-Earth3P-HR (ecearth), and HAdGEM3-GC31-HM (hadgem). Each model has a corresponding set of synthetic TCs[32]. The STORM dataset was subset to only include cyclones whose tracks come within 150 km of any floodplain node of the computational mesh. Following this subsetting, the pc scenario included 283 storms; cmcc included 175 storms; cnrm included 163 storms; ecearth included 363 storms; and hadgem included 233 storms. Figure 6 shows both

Table 3 | Return periods of the most extreme modeled storm-tide from historical storms at each study site under all scenarios

Site	Storm	Storm-tide (m)	Return period (years)				
			pc	cnrm	cmcc	ecearth	hadgem
Madras Atomic Power Station	Thane	1.20	70	80	60	50	50
Kovvada Atomic Power Project	Hudhud	1.71	1190	230	350	60	90
Gangamati	Sidr	5.08	180	1850	3250	1030	950
Mazher Char	Aila	2.57	70	70	140	50	60
Boyar Char	Sidr	3.61	80	120	520	100	110
Tazumuddin	Sidr	3.19	70	90	280	70	90
Galachipa	Sidr	4.12	100	320	1180	260	280
Kuakata	Sidr	4.97	210	1730	3340	780	880

Return periods are rounded to the nearest decade.

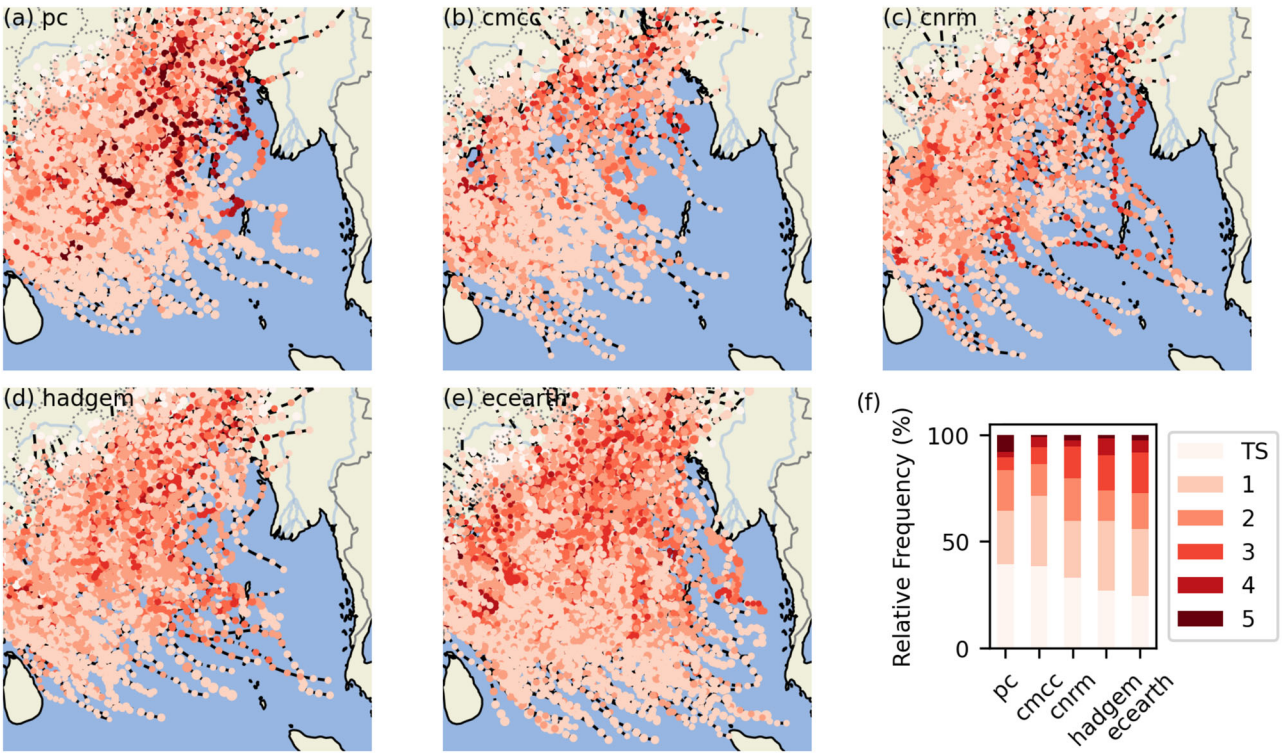

Fig. 6 | Visualization of STORM synthetic tropical cyclone tracks used in the full model ensemble. a–e show the subset of STORM tracks for pc, cmcc, cnrm, hadgem, and ecearth climate scenarios, respectively. Each individual track is plotted with the white-to-red dots indicating the severity of the storm at that point. **f** shows the relative frequency of the maximum storm category on the Saffir–Simpson scale of the subset of storms.

the tracks of the subset of STORM as well as the relative frequency of the maximum category of each storm.

Surface wind and atmospheric pressure fields are reproduced from STORM track data using a parametric cyclone model. For this study, the model described in ref. 46 (hereafter CLE15) was used due to its superior performance as described in ref. 47. Background winds fields are calculated with the model of ref. 48. In addition to the values of maximum velocity (V_{max}), radius of maximum winds (R_{max}), and minimum pressure (P_{min}) provided by the STORM dataset, the CLE15 model has free parameters c_k, c_d, and w_{cool}. c_k and c_d are the exchange coefficients of enthalpy and momentum respectively and, in this study, are calculated from the parametric relationship $c_k/c_d = 0.00055V_m^2 - 0.0259V_m + 0.763$[49]. w_{cool} is the magnitude of the radiative-subsidence rate in the free troposphere and has been estimated from climatology to be ≈2 mm s^{-1}. The LC12 "background" wind field accounts for the translation component of surface wind from a moving TC[48]. determined that a background wind reduction factor of 0.55 and a rotation of 20° best matched observed wind fields from TCs.

Tidal forcing in the model comes from both the equilibrium tide forced at every node in the model and from enforcing tidal boundary conditions at the open ocean boundary in the south of the domain. Tidal elevations for the boundary are obtained from the TPXO9-atlas version 2[50]. Both the boundary condition and the equilibrium tide were forced using the major 8 constituents (M_2, Q_1, O_1, P_1, K_1, N_2, S_2, and K_2).

In order to account for the impact of tidal stage when a TC makes landfall, each member of the STORM dataset was run at four different tidal stages: (1) high tide at landfall; (2) low tide at landfall; (3) maximum along-storm velocity at landfall; and (4) minimum along-storm velocity at landfall. These tidal conditions were calculated at the nearest computational node to the point where the TC makes landfall in the model. This methodology helps to account for the nonlinear impacts that tides can have on storm surge[51].

The effect of riverine discharge on water levels is accounted for by including two major rivers as inflow conditions at the model boundary. These two rivers are the Meghna and Padma rivers. Due to the location of the northern model boundary, this condition captures the flow from the three major tributaries of the GBM delta. Riverine discharge is from the Global Flood Awareness System (GloFAS)[33]. GloFAS data covering the time period 1979 through 2022 at daily frequency were averaged on a monthly basis (mean monthly flow). For each month, three different flow conditions were considered: (1) maximum mean monthly flow; (2) mean mean monthly flow; and (3) minimum mean monthly flow.

In order to account for the impact of mean sea level rise on coastal water levels, a persistent offset derived from the Deltares Global Tide and Surge Model (GTSM) version 3.0[34] was applied at the open ocean boundary of the model. For the pc scenario, no mean sea level adjustment was applied since the bathymetry from which the numerical mesh was created is referenced to present-day mean sea level. For future conditions, the mid-century (2050) mean sea level rise was interpolated from the GTSM output and added at the open ocean boundary. The mean sea level (η_{msl}) in Eqs (1) and (2) is calculated as the zero-phase constituent from the auxiliary simulations resulting from this additional offset at the boundary. It is critical to note that the GTSM model does not include the effects of land subsidence on mean sea levels[10]. estimates that the GBM delta is subsiding at rates between 1 and 7 mm per year, which would affect flooding levels in the region.

Computational mesh development and setup

The computational mesh used in this study was created using OceanMesh2D[52], a MATLAB toolbox designed to create unstructured meshes for coastal domains. As can be seen in Fig. 1, the model covers the majority of the BoB, including the eastern coast of India and the Ganges River Delta. The mesh resolution ranges from 25 km in the deep-ocean to 500 m in coastal zones and on floodplains. OceanMesh2D determines target resolution via a number of parameters designed to ensure that the mesh adequately resolves bathymetric/topographic features. A "one-step" procedure was used to generate the mesh, wherein both the ocean and floodplain portions of the mesh are created simultaneously in order to ensure a smooth transition from ocean to land within the computational domain. Bathymetry for the model was interpolated primarily from GEBCO2020[53]. Additionally, the oceanic portion of the bathymetric dataset described in ref. 12 was included to improve results along the coast of Bangladesh. Topography was interpolated from the SRTM15+ dataset[54]. Bathymetry and topography were modified via a "pit-filling" algorithm to help with the numerical stability of the wetting and drying algorithm.

The model uses parameterizations of both boundary layer dissipation and internal tide dissipation. Bottom friction is calculated using Manning's n converted to bottom-drag coefficients using the relationship $c_d = (gn^2)/H^{1/3}$, where c_d is the drag coefficient, g is acceleration due to gravity, n is Manning's n coefficient, and H is the total water column height. Internal tide dissipation is included using a modified[55] parameterization that is a function of local bathymetric slopes and density gradients[56,57]. Bathymetric slopes are calculated from GEBCO2020 data using a cell-averaged approach.

Hydrodynamic solutions are often sensitive to dissipation, motivating the determination of an approximately optimal spatial distribution of coefficients for internal tide and bottom friction[57]. To this end, we divided the model domain into independent regions for Manning's n and internal tide, where the vertices in each region are assigned a single value for the coefficient. 100 Manning's n regions were generated using a k-means clustering algorithm, which grouped mesh vertices based on location, bathymetric depth (>0 m), and seabed lithology[58,59]. Separately, 10 internal tide dissipation regions were generated based on location, bathymetric depth (>1 km), and bathymetric slope. Using the Stochastic reduced-order Models with Python (SROMPy) library[60], 100 randomized samples of combinations of Manning's n and internal tide coefficient values were generated. For each sample, a tide-only simulation was performed, and the mean discrepancy (Eq. (3)) compared to tide gauges in the region was assessed. By using a functional minimization technique from SciPy[61], the optimal (given the arrangement of regions and tidal error metric) friction coefficients were estimated. Note that overland Manning's n values were excluded from this process and instead calculated from the Global Land Cover Characterization database[62] based off of recommended values from the National Land Cover Database[63].

Model validation

In order to assess the skill of the numerical model in accurately capturing extreme water levels, hindcasts assessing the accuracy of both tides and surge caused by historical cyclones were performed.

For tidal validation, a tide-only simulation forced with the 8 major constituents was performed. The model was given 10 days to "spin-up" and a harmonic analysis was performed using UTide[64] on 354 days of water levels at stations. Comparisons are made between modeled tidal amplitudes and phases and those from the following observations: pelagic DART buoy 23401[65]; coastal tide gauges from the Global Extreme Sea Level Analysis dataset version 3[66] (GESLAv3); and coastal stations used in the validation of the models described in refs. 12,15. In order to assess both the amplitude and phase errors simultaneously, the root mean square discrepancy[67] (D) was calculated for the dominant lunar constituent (M_2); a combination of four major constituents (M_2, S_2, K_1, and O_1); and the combination of all 8 major constituents. D is calculated as:

$$D = \sqrt{0.5 \sum_k \left[\left(A_o^k\right)^2 + \left(A_m^k\right)^2 - 2A_o^k A_m^k \cos\left(\theta_o^k - \theta_m^k\right) \right]} \quad (3)$$

Where A and θ are amplitude and phase, the superscript k denotes the kth constituent, and the subscripts o and m denote observed and modeled, respectively. Mean values across all stations are 14.68, 16.74, and 14.71 cm for M_2, 4 constituents, and 8 constituents, respectively. The 4 constituent error value is larger than the 8 constituent because of the inclusion of tide gauges where only 4 constituents are publicly available. When only stations with observational data for all 8 constituents are included in the calculation of error statistics the mean error values are 12.29, 14.09, and 14.71 cm. Full error statistics across all stations can be found in Table S1. Figure S1 shows scatter plots of the amplitude and phase errors.

Model simulations are compared against water level observations for TCs in the historical record (Fig. 7c). The best track data for each storm were retrieved from the Joint Typhoon Warning Center (JTWC) Best Track Archive. Like the STORM dataset, the parameters available in the best track archive can be used to compute wind and pressure fields using the CLE15+LC12 model. Each storm was simulated using the TPXO9-atlas tidal forcing and GloFAS riverine forcing consistent with the time of the storm. Both event maximum storm-tide—defined as the total water level incorporating the impact of meteorology, tides, and riverine flow—and storm surge—defined as the total water level minus the tidal water level, also called a non-tidal residual—of the model are compared to observations (Fig. 7a, b). Root mean square errors (RMSE) for maximum storm-tide and storm surge are 71 and 66 cm, respectively. Observations where the storm center came within 50–150 km of the station, as well as the extreme surges, are fairly well represented. The negative mean bias is mostly associated with further afield observations—e.g., storm-tide at Galachipa during Cyclone Amphan—where the parametric TC winds are too weak. Parametric models better capture peak winds near the center of a storm but do not necessarily resolve the external winds. When these same historical storms are simulated using a reanalysis wind product such as ERA5[37], stations that are further from the center of the storm are better captured (see Fig. S2). At the same time, ERA5 underestimates high-intensity TC winds and hence some of the larger water levels that we capture with the parametric model. Overall, given that the tidal results of the model are comparable to others for the region[12,15], and that the extreme surges are relatively well captured, we believe that these results provide adequate confidence in the model and, subsequently, the projections of long-term flood return periods.

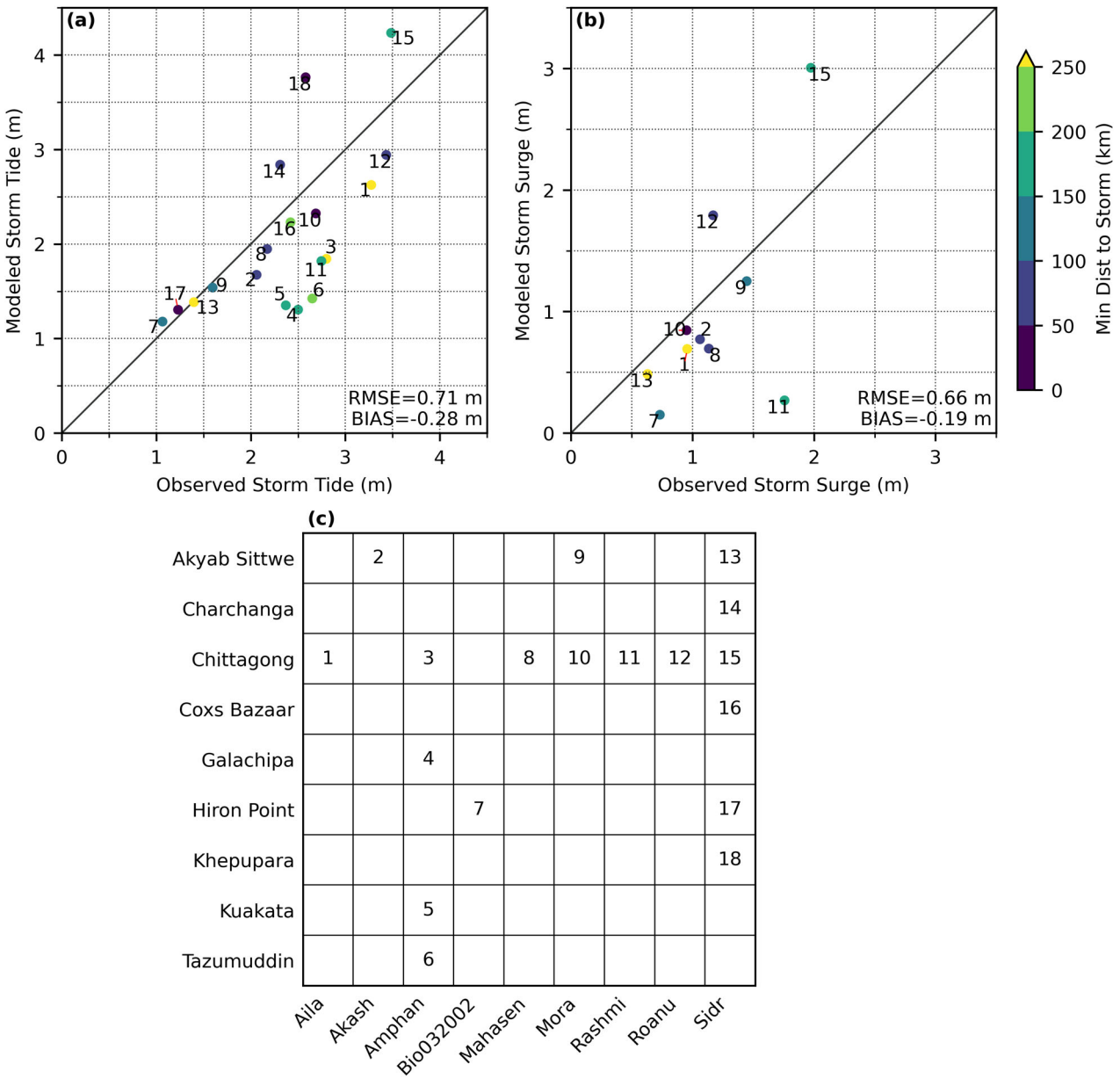

Fig. 7 | Validation data for the Bay of Bengal model comparing modeled and observed storm-tides and storm-surges. a Modeled versus observed event-maximum storm-tides for stations with available observations in the model domain. **b** Modeled versus observed event-maximum storm-surges for stations with available data in the model domain. **c** Station/Storm observation availability matrix. The number labels in (**a**, **b**) correspond to the values in (**c**). For example, point (1) in both (**a**, **b**) shows the storm-tide (storm-surge) at Chittagong caused by Cyclone Aila. The colors of points in (**a**, **b**) denote the minimum distance from the storm track to the station.

Extreme value analysis methodology

Each 1000 year period (pc, cmcc, cnrm, ecearth, and hadgem) was sampled separately with replacement 200 times. The peak storm-tide was taken as the highest water level from the ensemble member within 5 km of each site of interest. For each sample, one of the 12 storm perturbations (excluding the baseline case) was selected. Thus, for example, sample number 1 of the pc scenario might include: storm 1 with low tidal stage and minimum riverine flow, storm 2 with maximum along-storm tidal flow with maximum riverine flow, …, and storm 283 with high tidal stage and mean riverine flow. Sample number 12 of the hadgem scenario might include: storm 1 with high tidal stage and maximum riverine flow, storm 2 with low tidal stage and minimum riverine flow, …, and storm 233 with minimum along-storm tidal flow and maximum riverine flow. The resulting samples were individually fit using a Generalized Pareto Distribution (GPD) with peaks over threshold (POT)[68,69]. The GPD is commonly used to model the heavy tails of environmental extremes, including TC-driven coastal flooding[68,70]. The cumulative distribution function takes the form:

$$F(x) = \begin{cases} 1 - (1 - k\frac{x-\mu}{\sigma})^{1/k} & \text{for } k \neq 0 \\ 1 - e^{-\frac{x-\mu}{\sigma}} & \text{for } k = 0 \end{cases} \quad (4)$$

where,

k = shapeparameter
μ = locationparameter
σ = scaleparameter

To ensure that the GPD is properly fit to the tail of the distribution, POT is used to select only values in the sample greater than a given

threshold, $t \equiv \mu$. The best methodology for threshold selection is a widely discussed topic, with approaches ranging from graphical methods, to various goodness of fit tests, to parameter stability analyses[68,71]. Due to the large number of samples to be fit in this study, the automated methodology of ref. 72 was adopted. This approach uses the modified Anderson Darling (A_R^2) test[73] and p-value minimization to find the "best" threshold. A_R^2 is calculated as:

$$A_R^2 = \frac{n}{2} - \sum_{i=1}^{n}\left[\left(2 - \frac{2i-1}{n}\right)\log(1-z_i) + 2z_i\right] \quad (5)$$

where x_i are sorted samples $x_1 \le x_2 \le \cdots \le x_n$, n is the number of samples and $z_i = F(x_i)$ are the probabilities that x_i was drawn from the parametric distribution $F(x)$ fit to the sample using the L-Moments method[74]. This method of estimating the shape, location, and scale parameters of a GPD is highly computationally efficient, greatly reducing the time required to fit large numbers of thresholds. Shape, location, and scale parameters are estimated as:

$$\begin{aligned} k &= (3t_3 - 1)/(1 + t_3) \\ \sigma &= I_2(1-k)(2-k) \\ \mu &= I_1 - \sigma/(1-k) \\ I_1 &= b_0 \\ I_2 &= 2b_1 - b_1 \\ I_3 &= 6b_2 - 6b_1 + b0 \\ t_3 &= \tfrac{I_3}{I+2} \\ b_k &= \tfrac{1}{n}\sum_{i=k+1}^{n} \tfrac{(i-1)(i-2)\cdots(i-k)}{(n-1)(n-2)\cdots(n-k)} x_i \end{aligned}$$

To account for the effect of sample size on the parametric fit, the complement of the p-value $(1 - p)$—where p is defined as the probability that a value greater than or equal to A_R^2 was drawn from a parametric distribution given shape parameter k and number of samples n—is minimized in favor of minimizing A_R^2. As shown in ref. 72, the distribution of A_R^2 calculated from a parametric distribution is insensitive to scale and location parameters. p-values were calculated via bootstrapping for $n \in [5, 363]$ and $k \in [-3.00, -2.99, -2.98, \ldots, 2.98, 2.99, 3.00]$.

The procedure used to calculate return levels for each scenario can be summarized as:

- Create 200 samples of η_{max} of the 1000 year period, randomly selecting a storm perturbation with replacement.
- For each sample j, sort the maximum water levels $\eta_{max,i}$ such that $\eta_{max,1} \le \eta_{max,2} \le \cdots \le \eta_{max,nstorms}$ where $nstorms$ is the number of storms for that scenario.
- Identify the potential thresholds (t_k) for sample j as the unique values of $\eta_{max,i}$.
- Perform a GPD fit using L-Moments for each t_k on the n values $\eta_{max,\,i} \ge t_k$.
- Calculate A_R^2 and $1 - p$ for each t_k. A_R^2 and $1 - p$ are functions of the estimated shape parameter and the number of points n used to perform the fit.
- Select t_k (and corresponding GPD parameters) that minimizes $1 - p$.
- From the 200 samples, calculate mean return periods and confidence intervals (via non-parametric bootstrapping) from each GPD fit.Figure S3 shows an example of fitting to one individual sample (steps 2–6).

Data availability

Data from this study is available in the Zenodo repository at https://doi.org/10.5281/zenodo.15539675. It contains (1) observation data used for tidal and historical TC validations, (2) the hydrodynamic model domain and mesh, and (3) modeled maximum water levels from all experiments (tidal validation, historical TC validation, historical synthetic TCs, and future synthetic TCs). The GEBCO 2020 dataset can be found at https://www.gebco.net/. SRTM15+ is available at https://doi.org/10.5069/G92R3PT9. GESLAv3 water levels are published in two parts at https://doi.org/10.5285/d21a496a-a48e-1f21-e053-6c86abc08512 and https://doi.org/10.5285/d21a496a-a48f-1f21-e053-6c86abc08512. Historical TC tracks are available from the JTWC website https://www.metoc.navy.mil/jtwc/jtwc.html. The STORM dataset for present condition synthetic tracks can be found at https://doi.org/10.4121/12706085.v4, while the future condition synthetic TC's are published at https://doi.org/10.4121/14237678.v2. GloFAS riverine discharge can be downloaded from https://doi.org/10.24381/cds.a4fdd6b9. GTSM mean sea level projections are available at https://doi.org/10.24381/CDS.A6D42D60.OceanMesh2D v6.0 is available at https://doi.org/10.5281/zenodo.2605380 under the Creative Commons Attribution 4.0 International license. The coupled ADCIRC+SWAN model is available at https://github.com/adcirc/adcirc under the GNU General Public License Version 3. SROMPy is available at https://github.com/nasa/SROMPy, and the SciPy version 1.16.0rc library can be found at https://doi.org/10.5281/zenodo.15620045.

Received: 13 October 2025; Accepted: 28 January 2026;
Published online: 27 February 2026

References

1. Needham, H. F., Keim, B. D. & Sathiaraj, D. A review of tropical cyclone-generated storm surges: Global data sources, observations, and impacts. *Rev. Geophys.* **53**, 545–591 (2015).
2. Becker, M., Karpytchev, M. & Papa, F. Hotspots of relative sea level rise in the tropics. In (eds Venugopal, V., Sukhatme, J., Murtugudde, R. & Roca, R.) *Tropical Extremes*, Ch 7, 203–262 (Elsevier, 2019).
3. Ikeuchi, H. et al. Compound simulation of fluvial floods and storm surges in a global coupled river-coast flood model: model development and its application to 2007 Cyclone Sidr in Bangladesh. *J. Adv. Model. Earth Syst.* **9**, 1847–1862 (2017).
4. Saengsupavanich, C., Agarwala, N., Magdalena, I., Ratnayake, A. S. & Ferren, V. Impacts of a growing population on the coastal environment of the Bay of Bengal. *Anthr. Coasts* **7**, 24 (2024).
5. Reimann, L., Vafeidis, A. T. & Honsel, L. E. Population development as a driver of coastal risk: Current trends and future pathways. *Camb. Prisms Coast. Futures* **1**, e14 (2023).
6. Koks, E. E., Le Bars, D., Essenfelder, A., Nirandjan, S. & Sayers, P. The impacts of coastal flooding and sea level rise on critical infrastructure: a novel storyline approach. *Sustain. Resilient Infrastruct.* **8**, 237–261 (2023).
7. Mühlhofer, E., Bresch, D. N. & Koks, E. E. Infrastructure failure cascades quintuple risk of storm and flood-induced service disruptions across the globe. *One Earth* **7**, 714–729 (2024).
8. Ali, H., Fowler, H. J., Vanniere, B. & Roberts, M. J. Fewer, but more intense, future tropical storms over the Ganges and Mekong basins. *Geophys. Res. Lett.* **50**, e2023GL104973 (2023).
9. Syvitski, J. P. M. et al. Sinking deltas due to human activities. *Nat. Geosci.* **2**, 681–686 (2009).
10. Becker, M. et al. Water level changes, subsidence, and sea level rise in the Ganges-Brahmaputra-Meghna delta. *Proc. Natl. Acad. Sci. USA* **117**, 1867–1876 (2020).
11. Woodworth, P. L. et al. Towards a global higher-frequency sea level dataset. *Geosci. Data J.* **3**, 50–59 (2017).
12. Krien, Y. et al. Improved bathymetric dataset and tidal model for the northern Bay of Bengal. *Mar. Geod.* **39**, 422–438 (2016).
13. Gayathri, R., Murty, P. L. N., Bhaskaran, P. K. & Srinivasa Kumar, T. A numerical study of hypothetical storm surge and coastal inundation for AILA cyclone in the Bay of Bengal. *Environ. Fluid Mech.* **16**, 429–452 (2016).
14. Krien, Y. et al. Towards improved storm surge models in the northern Bay of Bengal. *Cont. Shelf Res.* **135**, 58–73 (2017).

15. Khan, M. J. U. et al. Towards an efficient storm surge and inundation forecasting system over the Bengal delta: chasing the Supercyclone Amphan. *Nat. Hazards Earth Syst. Sci.* **21**, 2523–2541 (2021).
16. Samiksha, V., Vethamony, P., Antony, C., Bhaskaran, P. & Nair, B. Wave-current interaction during Hudhud cyclone in the Bay of Bengal. *Nat. Hazards Earth Syst. Sci.* **17**, 2059–2074 (2017).
17. Sahoo, B. & Bhaskaran, P. K. A comprehensive data set for tropical cyclone storm surge-induced inundation for the east coast of India. *Int. J. Climatol.* **38**, 403–419 (2018).
18. Rao, A. D., Upadhaya, P., Pandey, S. & Poulose, J. Simulation of extreme water levels in response to tropical cyclones along the indian coast: a climate change perspective. *Nat. Hazards* **100**, 151–172 (2020).
19. Rao, A. D., Upadhaya, P., Ali, H., Pandey, S. & Warrier, V. Coastal inundation due to tropical cyclones along the east coast of India: an influence of climate change impact. *Nat. Hazards* **101**, 39–57 (2020).
20. Khan, M. J. U. et al. Storm surge hazard over Bengal delta: a probabilistic-deterministic modelling approach. *Nat. Hazards Earth Syst. Sci.* **22**, 2359–2379 (2022).
21. Leijnse, T. W. B., Giardino, A., Nederhoff, K. & Caires, S. Generating reliable estimates of tropical-cyclone-induced coastal hazards along the Bay of Bengal for current and future climates using synthetic tracks. *Nat. Hazards Earth Syst. Sci.* **22**, 1863–1891 (2022).
22. Qiu, J., Ravela, S. & Emanuel, K. From decades to years: rising seas and cyclones amplify Bangladesh's storm-tide hazards in a warming climate. *One Earth* **8**, 101273 (2025).
23. Pandey, S., Rao, A. D. & Haldar, R. Modeling of coastal inundation in response to a tropical cyclone using a coupled hydraulic HEC-RAS and ADCIRC model. *J. Geophys. Res. Oceans* **126**, e2020JC016810 (2021).
24. Murty, P. L. N., Rao, A. D., Srinivas, K. S., Rao, E. P. R. & Bhaskaran, P. K. Effect of wave radiation stress in storm surge-induced inundation: a case study for the east coast of India. *Pure Appl. Geophys.* **177**, 2993–3012 (2020).
25. Luettich, R. A. & Westerink, J. J. *ADCIRC: an Advanced Three-dimensional Circulation Model for Shelves Coasts and Estuaries, Report 1: Theory and Methodology of ADCIRC-2DDI and ADCIRC-3DL, Dredging Research Program*. DRP-92-6, (U.S. Army Engineers Waterways Experiment Station, 1992).
26. Pringle, W. J., Wirasaet, D., Roberts, K. J. & Westerink, J. J. Global storm tide modeling with ADCIRC v55: unstructured mesh design and performance. *Geosci. Model Dev.* **14**, 1125–1145 (2021).
27. Dietrich, J. C. et al. Performance of the unstructured-mesh, SWAN +ADCIRC model in computing hurricane waves and surge. *J. Sci. Comput.* **52**, 468–497 (2012).
28. Bloemendaal, N. et al. Generation of a global synthetic tropical cyclone hazard dataset using STORM. *Sci. Data* **7**, 40 (2020).
29. Knapp, K. R., Kruk, M. C., Levinson, D. H., Diamond, H. J. & Neumann, C. J. The International Best Track Archive for Climate Stewardship (IBTrACS): unifying tropical cyclone data. *Bull. Am. Meteorol. Soc.* **91**, 363–376 (2010).
30. Bloemendaal, N. et al. STORM IBTrACS present climate synthetic tropical cyclone tracks. 4TU.Centre for Research Data https://doi.org/10.4121/12706085.V4 (2022).
31. Eyring, V. et al. Overview of the Coupled Model Intercomparison Project Phase 6 (CMIP6) experimental design and organization. *Geosci. Model Dev.* **9**, 1937–1958 (2016).
32. Bloemendaal, N. et al. STORM climate change synthetic tropical cyclone tracks (2023).
33. Zsoter, E. River discharge historical data from the Global Flood Awareness System. ECMWF https://doi.org/10.24381/CDS.A4FDD6B9 (2019).
34. Copernicus Climate Change Service. Global sea level change time series from 1950 to 2050 derived from reanalysis and high resolution CMIP6 climate projections. ECMWF https://doi.org/10.24381/CDS.A6D42D60 (2022).
35. Bloemendaal, N. et al. A globally consistent local-scale assessment of future tropical cyclone risk. *Sci. Adv.* **8**, eabm8438 (2022).
36. Government of Bangladesh. Cyclone Sidr in Bangladesh: Damage, Loss, and Needs Assessment for Disaster Recovery and Reconstruction. https://www.gfdrr.org/sites/default/files/2275_CycloneSidrinBangladeshExecutiveSummary.pdf (2008).
37. Copernicus Climate Change Service. ERA5 hourly data on single levels from 1940 to present. Copernicus Climate Change Service (C3S) Climate Data Store (CDS) https://doi.org/10.24381/CDS.ADBB2D47 (2018).
38. Luettich, R. A. & Westerink, J. J. Formulation and Numerical Implementation of the 2D/3D ADCIRC Finite Element Model Version 44.XX. 74 https://adcirc.org/wp-content/uploads/sites/2255/2018/11/adcirc_theory_2004_12_08.pdf (2004).
39. Lynch, D. R. & Gray, W. G. A wave equation model for finite element tidal computations. *Comput. Fluids* **7**, 207–228 (1979).
40. Westerink, J. J. et al. A basin- to channel-scale unstructured grid hurricane storm surge model applied to Southern Louisiana. *Mon. Weather Rev.* **136**, 833–864 (2008).
41. Bunya, S. et al. A high-resolution coupled riverine flow, tide, wind, wind wave, and storm surge model for Southern Louisiana and Mississippi. Part I: model development and validation. *Mon. Weather Rev.* **138**, 345–377 (2010).
42. Hope, M. et al. Hindcast and validation of Hurricane Ike (2008) waves, forerunner, and storm surge. *J. Geophys. Res.* **118**, 4424–4460 (2013).
43. Zijlema, M. Computation of wind-wave spectra in coastal waters with SWAN on unstructured grids. *Coast. Eng.* **57**, 267–277 (2010).
44. Dresback, K. M., Kolar, R. L. & Dietrich, J. C. On the form of the momentum equation for shallow water models based on the generalized wave continuity equation. *Adv. Water Resour.* **28**, 345–358 (2005).
45. Smagorinsky, J. General circulation experiments with the primitive equations. I. The basic experiment. *Mon. Weather Rev.* **91**, 99–164 (1963).
46. Chavas, D., Lin, N. & Emanuel, K. A model for the complete radial structure of the tropical cyclone wind field. Part I: comparison with observed structure. *J. Atmos. Sci.* **72** 3647–3662 (2015).
47. Wang, S., Lin, N. & Gori, A. Investigation of tropical cyclone wind models with application to storm tide simulations. *J. Geophys. Res. Atmos.* **127**, e2021JD036359 (2022).
48. Lin, N. & Chavas, D. On hurricane parametric wind and applications in storm surge modeling. *J. Geophys. Res. Atmos.* **117**, https://doi.org/10.1029/2011JD017126 (2012).
49. Chavas, D. R. & Lin, N. A model for the complete radial structure of the tropical cyclone wind field. Part II: wind field variability. *J. Atmos. Sci.* **73**, 3093 – 3113 (2016).
50. Egbert, G. D. & Erofeeva, S. Y. Efficient inverse modeling of Barotropic ocean tides. *J. Atmos. Ocean. Technol.* **19**, 183–204 (2002).
51. Horsburgh, K. J. & Wilson, C. Tide-surge interaction and its role in the distribution of surge residuals in the North Sea. *J. Geophys. Res. Oceans* **112**, 1–13 (2007).
52. Roberts, K. J., Pringle, W. J. & Westerink, J. J. OceanMesh2D 1.0: MATLAB-based software for two-dimensional unstructured mesh generation in coastal ocean modeling. *Geosci. Model Dev.* **12**, 1847–1868 (2019).
53. GEBCO Bathymetric Compilation Group 2020. The GEBCO_2020 Grid - a continuous terrain model of the global oceans and land. British Oceanographic Data Centre, National Oceanography Centre, NERC, UK https://doi.org/10.5285/A29C5465-B138-234D-E053-6C86ABC040B9 (2020).
54. Tozer, B. et al. Global Bathymetry and Topography at 15 Arc Sec: SRTM15+. *Earth Space Sci.* **6**, 1847–1864 (2019).

55. Egbert, G. D. & Ray, R. D. Significant dissipation of tidal energy in the deep ocean inferred from satellite altimeter data. *Nature* **405**, 775–778 (2000).
56. Pringle, W. J., Wirasaet, D. & Westerink, J. J. Modifications to internal tide conversion parameterizations and implementation into Barotropic ocean models. Preprint at *EarthArXiv*, https://doi.org/10.31223/osf.io/84w53 (2018).
57. Blakely, C. P. et al. Dissipation and Bathymetric sensitivities in an unstructured mesh global tidal model. *J. Geophys. Res. Oceans* **127**, e2021JC018178 (2022).
58. Dutkiewicz, A., Müller, R. D., O'Callaghan, S. & Jónasson, H. Census of seafloor sediments in the world's ocean. *Geology* **43**, 795–798 (2015).
59. Pringle, W. J. et al. Finite-Element barotropic model for the Indian and Western Pacific Oceans: Tidal model-data comparisons and sensitivities. *Ocean Model.* **129**, 13–38 (2018).
60. Warner, J. E. Stochastic reduced order models with Python (SROMPy) (2018).
61. Virtanen, P. et al. SciPy 1.0: fundamental algorithms for scientific computing in Python. *Nat. Methods* **17**, 261–272 (2020).
62. Earth Resources Observation And Science (EROS) Center. Global land cover characterization (GLCC) (2017).
63. Dewitz, J. National Land Cover Database (NLCD) 2019 Products (ver. 3.0, February 2024) (2024).
64. Codiga, D. L. Unified Tidal Analysis and Prediction Using the UTide Matlab Functions. **59** https://doi.org/10.13140/RG.2.1.3761.2008 (2011).
65. Stammer, D. et al. Accuracy assessment of global barotropic ocean tide models. *Rev. Geophys.* **52**, 243–282 (2014).
66. Haigh, I. D. et al. GESLA Version 3: A major update to the global higher-frequency sea-level dataset. *Geosci. Data J.* **10**, 293–314 (2022).
67. Wang, X., Chao, Y., Shum, C. K., Yi, Y. & Fok, H. S. Comparison of two methods to assess ocean tide models. *J. Atmos. Ocean. Technol.* **29**, 1159–1167 (2012).
68. Coles, S. *An Introduction to Statistical Modeling of Extreme Values*. Springer Series in Statistics (Springer, 2001).
69. Castillo, E. & Hadi, A. S. Fitting the generalized Pareto distribution to data. *J. Am. Stat. Assoc.* **92**, 1609–1620 (1997).
70. Lin, N., Emanuel, K. A., Smith, J. A. & Vanmarcke, E. Risk assessment of hurricane storm surge for New York City. *J. Geophys. Res. Atmos.* **115**, 2009jd013630 (2010).
71. Langousis, A., Mamalakis, A., Puliga, M. & Deidda, R. Threshold detection for the generalized Pareto distribution: review of representative methods and application to the NOAA NCDC daily rainfall database. *Water Resour. Res.* **52**, 2659–2681 (2016).
72. Solari, S., Egüen, M., Polo, M. J. & Losada, M. A. Peaks over threshold (POT): a methodology for automatic threshold estimation using goodness of fit p-value. *Water Resour. Res.* **53**, 2833–2849 (2017).
73. Sinclair, C., Spurr, B. & Ahmad, M. Modified Anderson Darling test. *Commun. Stat. Theory Methods* **19**, 3677–3686 (1990).
74. Hosking, J. R. M. & Wallis, J. R. *Regional Frequency Analysis: An Approach Based on L-Moments*, 1 edn (Cambridge University Press, 1997).

Acknowledgements

This study was supported by the Laboratory Directed Research and Development (LDRD) Program at Argonne National Laboratory through the U.S. Department of Energy (DOE). Argonne National Laboratory is operated for the U.S. DOE by UChicago Argonne LLC under Contract DE-AC02-06CH11357. We gratefully acknowledge the computing resources provided on Bebop and Improv high-performance computing clusters operated by the Laboratory Computing Resource Center at Argonne National Laboratory, used to conduct hydrodynamic model simulations.

Author contributions

All authors contributed to the conceptualization of this study. W.J.P. and V.R.K. were responsible for project administration and supervision. C.P.B. and W.J.P. both worked on methodology, resource acquisition (primarily computing time), and software. C.P.B. performed the simulations and formal analysis with input from both W.J.P. and V.R.K. C.P.B. wrote the original draf,t and all authors reviewed and edited the manuscript.

Competing interests

The authors declare no competing interests.

Additional information

Supplementary information The online version contains supplementary material available at https://doi.org/10.1038/s44304-026-00175-x.

Correspondence and requests for materials should be addressed to Coleman P. Blakely.